Journal of Food Engineering 305 (2021) 110598

Contents lists available at ScienceDirect

Journal of Food Engineering

journal homepage: http://www.elsevier.com/locate/jfoodeng

Rheology of cocoa butter

Kim Mishra [a,*], Lucas Kohler [a], Nico Kummer [a,b], Simon Zimmermann [a], Silas Ehrengruber [a], Fabian Kämpf [a], Damien Dufour [a], Gustav Nyström [a,b], Peter Fischer [a], Erich J. Windhab [a]

[a] Institute of Food, Nutrition and Health, ETH Zürich, Schmelzbergstrasse 9, 8092, Zürich, Switzerland
[b] Laboratory for Cellulose & Wood Materials, Empa – Swiss Federal Laboratories for Materials Science and Technology, Überlandstrasse 129, 8600, Dübendorf, Switzerland

ARTICLE INFO

Keywords:
Rheology
Thixotropy
UVP-PD in-line rheometry
Capillary rheometry
$\beta_{V/VI}$ cocoa butter
Herschel-Bulkley fluid
Crystal-melt suspension
Fractal dimension
Jammed suspension
Single crystal AFM

ABSTRACT

The rheology of $\beta_{V/VI}$ cocoa butter crystal melt suspensions (CB CMS) was investigated directly after crystallization using in-line capillary rheometry (UVP-PD) as well as after tempering at zero deformation using off-line capillary rheometry (CR) and rotational rheometry (RR). CB CMS thixotropy was quantified by RR revealing that structure build up processes at zero deformation were not at equilibrium after 18 h, whereas structure decay occurred mainly in the first 10 s of measurement at $\dot{\gamma} = 60\ s^{-1}$. CR and UVP-PD were identified as preferable methods to probe thixotropic materials due to the short measurement time t_M and uniform sample deformation history for every $\dot{\gamma}$-step. The scaling of the relative viscosity η_{rel} and the (apparent) yield stress τ_0/τ_0^{app} as function of deformation history revealed two different regimes. Directly after the crystallization, the CB CMS behaved like a suspension of anisotropic crystals with a fractal dimension $D \approx 1.57$, an intrinsic viscosity $[\eta]$ of 20 and a maximal packing fraction Φ_{max} of 0.17 leading to a scaling of $\eta_{rel} = (1 - (\Phi_{SFC}/\Phi_{max}))^{-3.4}$. After tempering at zero deformation, crystal aggregation increased the fractal dimension to $D = 2.6$ and the scaling of the relative viscosity η_{rel} reduced to $\sim \Phi_{SFC}^2$, analogously to a jammed system of elastic particles.

1. Introduction

Cocoa butter (CB) is a complex fluid exhibiting thixotropy, shear thinning and a crystal-melt equilibrium. It is the most relevant fat in the confectionery industry and has attracted the attention of scientists over the past 50 years due to its unique polymorphic behavior (Timms, 1984). Wille and Lutton (1966) defined six polymorphic forms (I-VI) with increasing melting temperature for CB. Many studies investigating the relationship between the polymorphic form of CB and chocolate properties such as fat bloom, snap, gloss and mouthfeel have adapted this nomenclature (Andrae-Nightingale et al., 2009; Aronhime et al., 1988; Chapman et al., 1971; Koyano et al., 1990; Svanberg et al., 2013). They identified β_V as the preferable polymorphic form which is responsible for the desired organoleptic properties of the final chocolate product. The identification of β_V as preferred crystal polymorph led to the development of tempering protocols, where combinations of crystallization temperature and shear rate $\dot{\gamma}$ were used to selectively produce crystals of the $\beta_{V/VI}$ polymorph (Bolliger et al., 1998; Padar et al., 2009). The tempering protocols were integrated into a fully automatized crystallization loop where CB crystal-melt suspensions (CMS) with crystals prevalent in the $\beta_{V/VI}$ polymorphic form could be produced as seeding suspensions for the cooling step in the chocolate production process (Birkhofer et al., 2008; Grob et al., 2021). Such crystals of the β polymorphic form were also shown to form networks at the oil/air interface and stabilize lipid foams (Mishima et al., 2016; Mishra et al., 2020a). To gain more information on the rheological behavior of $\beta_{V/VI}$ CB CMS, an in-line rheological measurement track based on the ultrasound velocity profile - pressure difference (UVP-PD) method was built (Birkhofer et al., 2008). This allowed for the transient measurement of the shear dependent viscosity $\eta(\dot{\gamma})$ as well as the Herschel-Bulkley model parameters, namely the flow exponent n, the consistency factor K as well as the yield stress τ_0 (Herschel and Bulkley, 1926). Despite the various studies on the crystallization of CB, there are no comprehensive models which relate crystal concentration and polymorphic form with the shear rheology of CB CMS. Most studies perform oscillatory shear experiments to obtain the rheological fingerprint of CB CMS (Macias-Rodriguez and Marangoni, 2018; Macias-Rodriguez et al., 2018; Pérez-Martínez et al., 2007). Such studies allow to draw conclusions on the rheological

* Corresponding author.
E-mail address: kim.mishra@hest.ethz.ch (K. Mishra).

https://doi.org/10.1016/j.jfoodeng.2021.110598
Received 24 November 2020; Received in revised form 23 January 2021; Accepted 17 March 2021
Available online 31 March 2021

properties at small deformations which relate to the fractal dimension D of the crystal network (Marangoni and Rogers, 2003; Narine and Marangoni, 1999). The fractal dimension dictates the scaling behavior of the rheological properties as function of crystal volume fraction. In typical shear crystallizers, CB CMS are subjected to large deformations and correspondingly high shear rates. It remains unclear whether the same fractal dimensions deduced at low deformations are applicable at such large deformations (Stranzinger et al., 2001, 2002). In this work, three methodologies to measure shear rheological properties of $\beta_{V/VI}$ CB CMS are presented. Firstly, in-line capillary rheometry by means of UVP-PD is shown. UVP-PD covers the highly dynamic low crystal content regime accessed by a direct crystallization process using a scraped surface heat exchanger (SSHE). Secondly, off-line capillary rheometry (CR) is discussed. CR covers the high crystal content regime accessed by tempering of the CB CMS at zero deformation for 18 h. Thirdly, a rotational rheometer (RR) measurement protocol to bridge the gap between in-line and off-line measurements is suggested. Lastly, rheological scaling laws as function of CB CMS crystal concentration are derived and supported by polarized light- (PLM) and atomic force microscopy (AFM) measurements.

2. Materials and methods

2.1. Cocoa butter (CB)

CB was kindly donated by Chocolat Frey AG (Buchs AG, Switzerland). Countries of origin are Nigeria, Cameroon, Ivory Coast and Ghana. The fatty acids were 61.5 w/w% saturated, 35 w/w% monounsaturated and 3.5 w/w% polyunsaturated. The CB was molten at 45 °C to erase all crystallization memory before being crystallized.

2.2. Crystallization

In-line capillary rheometry (UVP-PD): Crystallization was performed with a SSHE (Schröder GmbH & Co KG, Lübeck, Germany) at 1000 rpm corresponding to $\dot{\gamma} = 2150\ s^{-1}$ (Mishra et al., 2020b). Using a MS25-HT/P water bath (Julabo Labortechnik GmbH, Seelbach, Germany) with 3.2 kW cooling capacity the double mantled stator was tempered within a temperature range of 3–15 °C. Mass flow rate was varied between 800 and 1200 g min^{-1}. The stator diameter $2R_o$ measured 60 mm with a length of 400 mm. The rotor with two blades had a diameter $2R_i$ of 57 mm and was tempered at 32 °C with a Julabo F32 water bath (Julabo Labortechnik GmbH, Seelbach, Germany). An eccentric worm-drive pump (Allweiler GmbH, Radolfzell, Germany) pumped the liquid CB at 45 °C from the double mantled stainless steel vessel through double mantled and tempered 25 mm pipes into the gap between stator and rotor. *Off-line capillary rheometry:* CB was crystallized using the SeedMaster Cryst (Bühler AG, Switzerland). A schematic overview of the SeedMaster Cryst with the used settings is depicted in Figure S1. The CB was held at 45 °C prior to crystallization. During crystallization, the tank temperature was lowered to 26 °C and the CB was pumped by an excentrical screw pump (Netzsch Mohnopumpen GmbH, Waldkraiburg, Germany) through the SSHE at a mass flow rate of 33.4 kg/h and back into the tank. The SSHE rotated at 900 rpm with $2R_o = 60$ mm and $2R_i = 50$ mm, corresponding to $\dot{\gamma} = 617\ s^{-1}$. Stator wall temperature was held at 15 °C. This crystallization loop continued for 150 min reaching a final solid fat content (Φ_{SFC}) of about 13%. The CB CMS was then ripened at 31.5 °C in the stirred tank by a looped flow from the bottom to the top of the tank.

2.3. Crystallography

For both sampling modes the following procedures were used for crystallographic measurements:

2.3.1. In-line capillary rheometry (UVP-PD)

Samples were continuously produced at 10 °C SSHE stator wall temperature with 20 kg/h mass flow rate. A liquid nitrogen (LN_2) bath was used to quench crystallization. Small amounts of the product stream were dropped directly into the LN_2 bath to ensure rapid and uniform cooling. Subsequently, samples were transferred to a dry ice box prior to analysis and handled with precooled instruments.

2.3.2. Off-line capillary rheometry (CR)

Samples were transported in a temperature controlled and hermetically sealed box (TC-14FL-AC, Dometic Switzerland AG, Rümlang, Switzerland).

2.3.3. Melting curve determination

A differential scanning calorimeter (DSC) (dsc822e, Mettler Toledo GmbH, Greifensee, Switzerland) was used to investigate the melting behavior of CB CMS. For each sample, triplicates were measured. Sample weight was 5 ± 0.2 mg for every triplicate. Samples were put in 40 µl aluminum crucibles (Mettler Toledo GmbH, Switzerland) that weighted 50.49 ± 0.2 mg. Heat flow at a given temperature was evaluated using the STARe-Software (SW 8.1, Mettler Toledo GmbH, Greifensee, Switzerland). Results are displayed in Figure S2.

2.3.4. Polymorphic crystal form determination

An X-ray diffractometer (D8 advanced, Bruker GmbH, Karlsruhe, Germany) was used to characterize the CB CMS. The diffractometer radiation source was Cu-Kα1 with a wavelength of $\lambda = 0.15406$ nm and $E_{beam} = 40$ keV. The diffraction angle 2θ was set between 15° and 25/29° with a step size of 0.02° and a step duration of 1 s. Samples were rotated during the measurement. Results are displayed in Figure S2.

2.4. Solid fat content (Φ_{SFC}) determination

Φ_{SFC} was measured by pulsed nuclear magnetic resonance spectroscopy using a 20 MHz (0.47 T) minispec mq20 (Bruker Biospin, Fällanden, Switzerland) in the direct mode. The device was calibrated using paraffin–acrylic standards. Tempered glass tubes with an inner diameter of 1 cm, a wall thickness of 0.06 cm and a height of 18 cm were filled with 3–4 cm of sample and immediately analysed as described previously (Breitschuh and Windhab, 1996). Analyses were performed in triplicate. For both sampling modes the following procedures were taken: *In-line capillary rheometry (UVP-PD):* Samples were taken directly from the pipe exit. For highly viscous samples a tempered syringe with a plastic tube was used to fill the glass tubes. *Off-line capillary rheometry (CR):* Samples were taken prior to the measurement directly from the tempered barrels.

2.5. Light microscopy

PLM (Leica DM6, Leica Microsystems AG, Heerbrugg, Switzerland) was used. Samples were were thinly deposited with a scalpel onto a glass slide and immediately analysed.

2.6. Atomic force microscopy

CB CMS was harvested from the SeedMaster Cryst and immediately dropped into acetone at a ratio of approximately 1:10. The mixture was homogenized 30 s with a rotor stator (Polytron PT-7100, Kinematica AG, Luzern, Switzerland) at 4000 rpm and passed through a 4–7 µm filter. The filter cake was carefully harvested wih a spatula and washed again with acetone before being filtered a second time through a 4–7 µm filter. The filter cake was harvested again and washed before being passed through a 1.2 µm filter. The filter cake was harvested and dried in a vacuum chamber for 3 h at 20 °C and 200 mbar to yield a CB CMS powder. A 200 µL droplet of 0.05% Polyethyleneimin (PEI) (Sigma Aldrich, 800 Da) in water was deposited on a freshly cleaved mica for 15

min and rinsed off with 1 mL MilliQ water and blown dry with pressurized air (Sebben et al., 2019). CB CMS powder was suspended in ice cold ethanol at 0.1 mg/mL using a sonication bath until the suspension was turbid. A 50 μL droplet of the CB CMS powder suspension was dropped onto the PEI coated mica for 60 s and then blown dry with pressurized air without a rinsing step. Tapping mode atomic force microscopy (AFM) was performed on a Bruker Icon 3 equipped with Bruker RTESPA-300 probes at 20 °C. Scans of different size were made at 1024 × 1024 pixel^2\ resolution and at a scan rate of 0.5 Hz. The image raw data was processed using Bruker NanoScope Analysis software.

2.7. UVP-PD measurement set up

The UVP-PD measurements were done directly after crystallization. Double mantled pipes with 15 mm diameter held at 24.6–27.6 °C were used to convey the CB CMS. The pressure difference was measured in a 3.29 m pipe section. A diaphragm pressure sensor (CC1020, Labom GmbH, Hude, Germany) with a measurement range of 1.0–1.4 bar absolute pressure was used at the beginning of the pipe segment in order to calculate the pressure difference against atmospheric pressure at the pipe exit. In between the pressure sensor and the end of the pipe segment a custom built polyvinyl chloride cell with inserted ultrasonic transducers was used to record the flow profile. Two 4 MHz transducers (Imasonic SAS, Voray-sur-L'Ognon, France) with an active diameter of 5 mm were placed at 60° and 90° angle with respect to the flow axis in order to determine the velocity profile across the pipe diameter and the speed of sound consecutively. The transducers were preferably operated at 3.75 MHz with a pulse repetition frequency of 750 Hz and 128 repetitions. The signals of the transducers were recorded with the UB-Lab device (Ubertone, Schiltigheim, France). During approximately 60 s a total of six averaged profiles were recorded for one process setting. This procedure was repeated three times for each process setting. Subsequently the profiles were deconvoluted (Flaud et al., 1997; Jorgensen and Garbini, 1974; Kagiyama et al., 1999) and fitted with the Herschel-Bulkley model. Fitting the Herschel-Bulkley model onto the measured velocity profile requires the plug radius R_p, flow index n and consistency factor K as fitting parameters:

$$\nu_{HB}(r) = \begin{cases} \frac{n}{n+1}\frac{\Delta P}{2L_p K}^{\frac{1}{n}}\left[\left(R-R_p\right)^{1+\frac{1}{n}} - \left(r-R_p\right)^{1+\frac{1}{n}}\right], & \text{if } r \geq R_p \\ \nu_{HB}\left(R_p\right), & \text{if } r < R_p \end{cases} \quad (1)$$

The fitted plug radius R_p is related to the pressure drop ΔP, pipe length L_p and the yield stress τ_0 as follows:

$$R_p = \frac{2\tau_0 L_p}{\Delta P} \quad (2)$$

Examples of measured flow profiles are presented in Figure S3. The piping and instrumentation diagram as well as the schematic drawing of the measurement track can be seen in Figures S4 and S5.

2.8. Off-line capillary rheometry

CB CMS was collected from the back flow pipe at the reservoir tank of the SeedMaster Cryst in 300 mL plastic beakers. CB CMS was then transferred into CR barrels with radius $R_B = 10$ mm using a tempered syringe. Barrels were sealed with rubber plugs and submerged into a water filled doublle wall beaker tempered by a Lauda ECO E 4S waterbath (Lauda DR. R. Wobser GmbH & CO. KG, Königshofen, Germany). Tempering was done for 18 h at 20, 25, 30.6, 31.6, 33.3 and 33.8 °C yielding 70.6 ± 0.3, 60.5 ± 0.3, 28.3 ± 1.4, 21.1 ± 0.5, 11.9 ± 1.3, 6.5 ± 0.5% Φ_{SFC}. The tempered barrels were mounted in the pretempered capillary rheometer (Rheograph 2002, Göttfert Werkstoff-Prüfmaschinen GmbH, Buchen, Germany). The temperature of the double jacketed barrel fitting was controlled using a Julabo F32 CH oil bath (Julabo Laborthechnik GmbH, Seelbach, Germany) with thermal oil (Thermal H10, Julabo Laborthechnik GmbH, Seelbach, Germany). Measurements were shear rate controlled (1000, 600, 360, 216, 129.8, 77.8, 46.6, 28.0, 16.8, 10.0, 6.00, 3.60, 2.20, 1.30, 0.80 s^{-1}) and run from highest to lowest shear rate. Shear rates were converted to ram velocities (V_{ram}) according to Equation (3):

$$V_{ram} = \frac{\dot{\gamma}_w^{app} R^3}{4R_B^2} \quad (3)$$

with $\dot{\gamma}_w^{app}$ being the desired apparent wall shear rate in the capillary, R the capillary radius and R_B the barrel radius. The maximum measuring time per $\dot{\gamma}$ step was set to 300 s. If the mean value of the pressure reading remained within a 5% tolerance for 30 s, the next $\dot{\gamma}$ step was introduced by the LabRheo program. The pressure for samples tempered at 20, 25, 30.6 and 31.6 °C were measured using a 50, 100 and 200 bar ± 0.25% melt pressure sensor (Dynisco, Franklin MA, USA). The pressure for samples tempered at 33.3 °C were measured using a 3.5 ± 1% bar pressure sensor (Kulite Semiconductor Products INC, New Jersey, USA). The pressure for samples tempered at 33.8 °C were measured using a 1.7 ± 1% bar pressure sensor (Kulite Semiconductor Products INC, New Jersey, USA). Data collection and control of the rheometer was done using the LabRheo 3.4.0 program (Göttfert Werkstoff-Prüfmaschinen GmbH, Buchen, Germany). For details on the evaluations and applied corrections see Figure S6-S12.

2.9. Rotational rheometry

A shear rate controlled rheometer (MCR 702, Anton Paar, Graz, Austria) was used. CB CMS was collected from the back flow pipe of the Seedmaster Cryst in 300 mL plastic beakers and immediately transferred into the Couette geometry (CC27, Anton Paar, Graz, Austria). There it was left to equilibrate at 33.8 °C for 10 min. Pre-shearing was performed at 1000 s^{-1} for 10 min before the resting interval t_R at zero deformation was initiated. *Shear rate ramps:* After a given time at rest t_R, a $\dot{\gamma}$-ramp from 1 to 1000 s^{-1} was performed with 5 measurement points of 10–20 s per decade. The sequence (1) pre-shearing, (2) time at rest t_R and (3) $\dot{\gamma}$-ramp was iterated for varying times at rest t_R. *Constant shear rate:* After t_R = 6.5 10^4 s an abrupt increase to $\dot{\gamma}$ = 60 s^{-1} was performed and maintained for 1000 s with a measurement interval of 1 s. All Measurements were performed in triplicates and averaged.

3. Results

Fig. 1 shows the shear viscosity η as function of the shear rate $\dot{\gamma}$ for CB CMS at various Φ_{SFC}. The UVP-PD technique was applied for in-line measurements performed directly after crystallization by SSHE. CR was applied to perform off-line measurements of samples crystallized in a loop and subsequently tempered in a water bath at zero deformation conditions. X-ray diffraction as well as DSC confirmed that the investigated CB CMS for in-line as well as off-line measurements were consisting of β_V and β_{VI} crystals (Figure S2). The main scattering peak of the CB CMS investigated at in-line conditions was slightly shifted (19.7°) compared to the samples investigated at off-line conditions (19.2–19.4°), indicating a higher prevalence of β_V crystals. Furthermore, the melting peak for the CB CMS investigated at in-line conditions was at slightly lower temperature (32.4 °C) than the CB CMS investigated at off-line conditions (34.3–35.3 °C), confirming the increased abundance of β_V crystals. Additionally, CB CMS investigated at off-line conditions showed additional melting peaks at lower temperatures due to the crystallization of the liquid fraction during cooling in the DSC. The UVP-PD technique was applicable up to 8.8 % Φ_{SFC}. At higher Φ_{SFC}, the absorption of the acoustic signal was impeding accurate velocity readings. A similar Φ_{SFC} range was previously reported for palm kernel oil (Mishra et al., 2020b). Shear rates of 0.1–100 s^{-1} were accessed depending on the investigated Φ_{SFC}. The CB CMS measured by UVP-PD showed shear

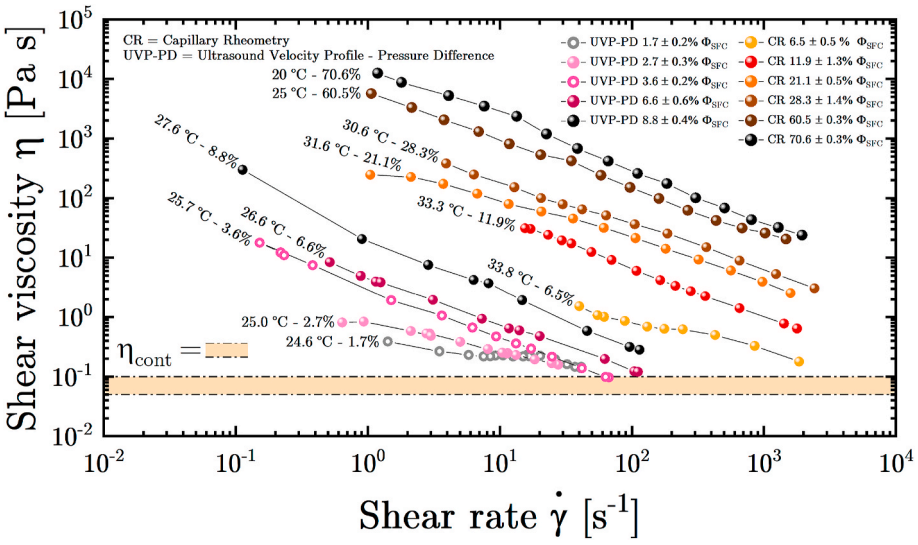

Fig. 1. The shear viscosity η as function of the shear rate $\dot{\gamma}$ for $\beta_{V/VI}$ CB CMS directly after crystallization (UVP-PD) and after tempering for 18 h (CR). Corresponding Φ_{SFC} are indicated next to the curves. Lines are inserted to guide the eye.

thinning behavior at all investigated Φ_{SFC}. With increasing Φ_{SFC}, higher η were reached and shear thinning more pronounced. Samples measured by off-line CR spanned Φ_{SFC} from 6.5 to 70.6%. The limiting factor for the lower $\dot{\gamma}$- and Φ_{SFC}- range was given by the pressure sensor accuracy. The CB CMS measured by CR showed shear thinning behavior at all investigated Φ_{SFC}. With increasing Φ_{SFC}, higher η were reached but shear thinning slopes remained similar between 11.9 and 70.6% Φ_{SFC}. Comparing the two methods in the narrow Φ_{SFC} range between 6.5 and 8.8 %, it becomes evident that the η measured by CR are higher than measured by UVP-PD. Regarding the shear thinning behavior, the two methods yield consistent results and a parallel shift to the right in the $\eta = f(\dot{\gamma})$ plane is observed. The increased η and the parallel shift to the right are a result of CB CMS deformation history. Below a critical deformation rate, the structure building forces, namely the crystal-crystal attractive forces, are stronger than the shear stress induced orientation forces. Consequently, if the CB CMS is deformed below the critical deformation rate, thixotropic rheological behavior occurs (Windhab, 1988). The zero deformation history prior to the CR measurements allowed for the stronger build up of an inner suspension structure compared to the non-zero deformation history prior to the UVP-PD measurements. However, once crystal-crystal bridges are disrupted, the mechanism of shear thinning due to crystal orientation in the flow field remains the same resulting in a parallel shift. RR was applied to quantify the structure build up as function of deformation history. The Couette geometry allows to accurately temper and simultaneously access high $\dot{\gamma}$. Figure 2 (A) shows the shear viscosity η as function of the shear rate $\dot{\gamma}$ for CB CMS measured by CR and RR. The measurement temperature of 33.8 °C for the RR was identical to the CR sample tempering corresponding to 6.5% Φ_{SFC}. Samples were left to rest between $t_R = 1.2\ 10^2$ and $t_R = 6.5\ 10^4$ s. With increasing t_R, the η of the flow curves increased thereby indicating structure build up. At low $\dot{\gamma}$, the η increase was more pronounced than at high $\dot{\gamma}$. For all rest times, the CB CMS measured by RR shows lower η compared to the CR data. Fig. 2(B) shows η as function of the measurement time t_M for CB CMS rested at $t_R = 6.5\ 10^4$ s and probed at $\dot{\gamma} = 60\ s^{-1}$. A rapid decrease of η as function of t_M in the first 10 s is visible. After the first 10 s, the decrease in viscosity slows down and asymptotically approaches an equilibrium value.

The high discrepancy of the CR compared to the UVP-PD and RR

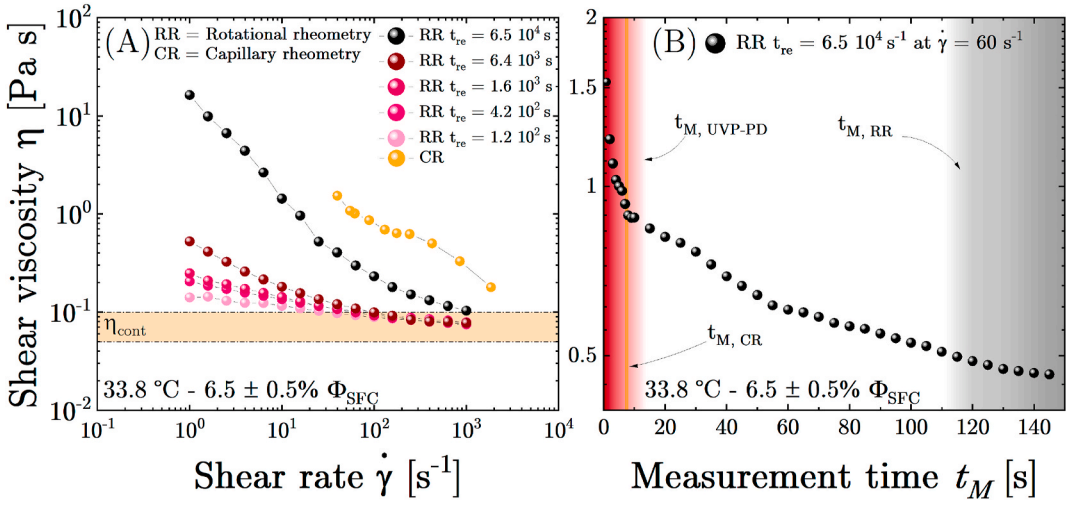

Fig. 2. (A) The shear viscosity η as function of the shear rate $\dot{\gamma}$ for 6.5% Φ_{SFC} CB CMS measured by CR and RR at 33.8 °C. RR measurements were performed with varying time at rest t_R. (B) The shear viscosity η as function of the measurement time t_M for CB CMS measured by RR at $\dot{\gamma} = 60\ s^{-1}$ after $t_R = 6.5\ 10^4$ s (18 h). The measurement was performed at 33.8 °C with measuring intervals of 1 s. For measurement time $t_M > 10$ s, rolling means of 5 points are displayed. Characteristic measurement times t_M for the UVP-PD, off-line CR and RR method used in this study are indicated.

derived viscosity curves as depicted in Figs. 1 and 2(A) are a consequence of measurement time difference between the two methods. Performing CR, the continuous flow of sample from barrel into die ensures identical deformation history for every $\dot{\gamma}$-step, whereas the batch probing in the RR alters the deformation history with every $\dot{\gamma}$-step. RR signal acquisition at a set $\dot{\gamma}$ occurs after a given criterion of stationarity, which typically leads to a t_M of 10–20 s per step. The CR signal acquisition depends on the sample residence time in the capillary, which is a function of the set $\dot{\gamma}$ and the capillary length. At $\dot{\gamma} = 60\ s^{-1}$, the CR measurement time $t_{M,CR}$ lies between 0 and 15 s and the RR measurement time $t_{M,RR}$ between 110 and 150 s including every shear step from $1\ s^{-1}$ to $60\ s^{-1}$ with 5 points per $\dot{\gamma}$-decade. Judging from Fig. 2(B), this difference in t_M causes substantially lower viscosity readings and explains the overlapping of the RR derived flow curves at high $\dot{\gamma}$. Comparing RR and CR derived results at the same t_M requires an analysis as performed in Fig. 2(B) for every $\dot{\gamma}$-step. This procedure is very time consuming, especially for increasing t_R. However, the RR method allows to determine thixotropic time scales with little effort, which is not the case for CR. The outlined methods show that the in-line measurement by UVP-PD most accurately accounts for the CB CMS deformation history for a given processing application. However, the measurable Φ_{SFC}- and $\dot{\gamma}$-range is limited. Off-line measurements by CR show little Φ_{SFC} limitations but are not suited for very low $\dot{\gamma}$. CR does not necessarily probe the CB CMS at a processing relevant deformation history. RR measurements are able to measure thixotropic time scales at low to intermediate Φ_{SFC} and for a wide range of $\dot{\gamma}$. Combining CR and RR measurements, we are able to correct for CB CMS deformation history at a wide range of Φ_{SFC} and $\dot{\gamma}$ thereby offering an alternative to in-line measurement methods.

The CB CMS thixotropy is a result of structural changes during CB CMS storage below the critical deformation rate. Structural changes affect rheological scaling properties as function of particle volume fraction. Investigating the rheological properties as function of crystal content allows us to draw conclusions on the fractal dimension D as well as the intrinsic viscosity $[\eta]$. From the fitting of the Herschel-Bulkley velocity for two dimensional pipe flow $\nu_{HB}(r)$ onto the measured velocity profile by UVP, estimates of the yield stress τ_0, the consistency factor K and the flow index n were derived. The $\tau = f(\dot{\gamma})$ data obtained by CR was fitted by a power-law function yielding K and n. The apparent yield stress τ_0^{app} was obtained by extrapolating the linear regression of the $\tau = f(\dot{\gamma})$ function to $\dot{\gamma} = 0$ as depicted in Figure S6(A) similar to previous studies on yield stress fluids (Bertsch et al., 2019b, a). The results are summarized in Fig. 3 (A-D). The two different slopes for τ_0, $\tau_0^{app} = f(\Phi_{SFC})$ in Fig. 3(A) are in accordance with literature (Awad et al., 2004; Marangoni and McGauley, 2003; Narine and Marangoni, 1999; Shih et al., 1990; Vreeker et al., 1992). At low crystal concentrations as measured by UVP-PD, the strong-link regime (SLR) is applicable. Since inter-crystal aggregate forces are *stronger* than intra-crystal aggregate forces, the scaling exponent is higher and originates from the single crystal properties. The scaling exponent can be related to the fractal dimension as follows (Awad et al., 2004; Marangoni and McGauley, 2003; Narine and Marangoni, 1999; Shih et al., 1990; Vreeker et al., 1992):

$$\tau_0 = b_{\tau S}\Phi_{SFC}^{(d+x)/(d-D)} \tag{4}$$

where $b_{\tau S}$ is a sample specific coefficient in Pa, d the Euclidean dimension, x the backbone fractal dimension of the crystals and D the fractal

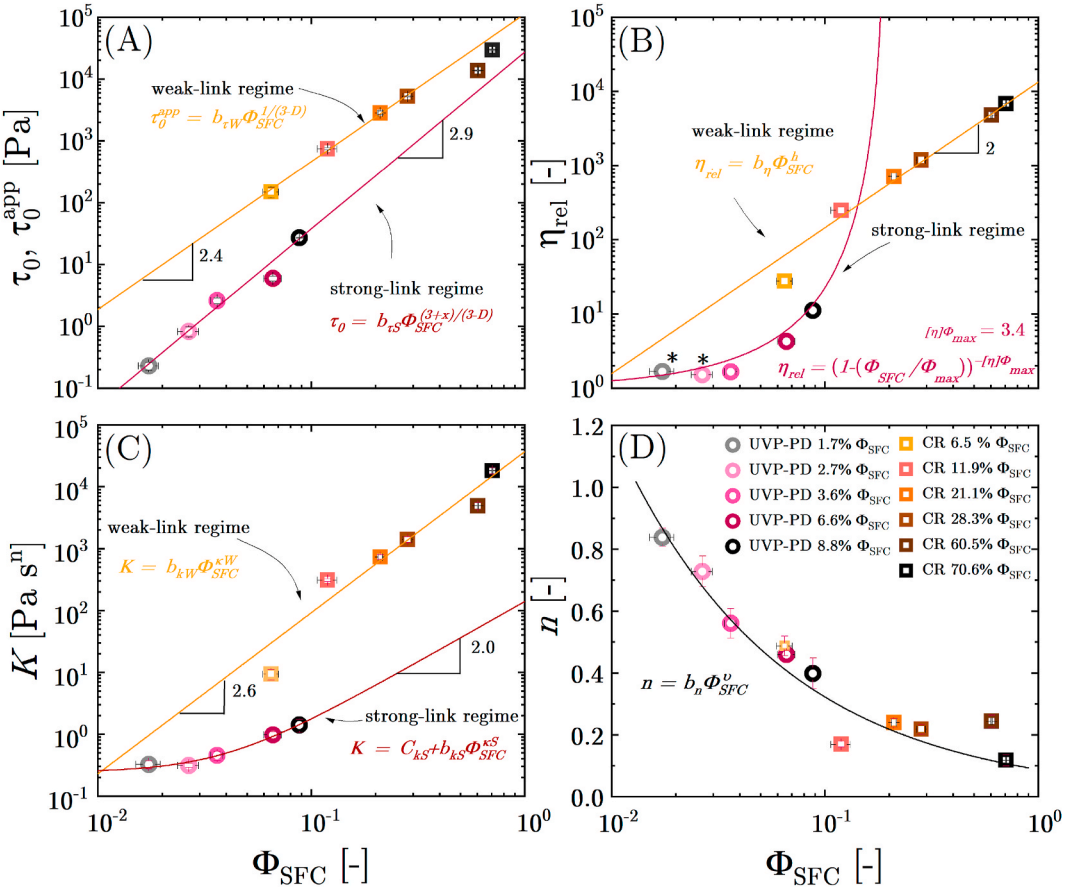

Fig. 3. (A) the (apparent) yield stress τ_0, τ_0^{app}, (B) the relative viscosity η_{rel} at $\dot{\gamma} = 40\ s^{-1}$ ($\eta_{\dot{\gamma}=40s^{-1}}/\eta_{cont}$), (C) the consistency factor K and (D) the flow exponent n as function of the CB CMS Φ_{SFC}. UVP-PD (circles) as well as CR measured (squares) samples are displayed. In (B), viscosities which were extrapolated to $\dot{\gamma} = 40s^{-1}$ are marked with a star.*

dimension of the crystals. Solving Equation (4) for $d = 3$ and $x = 1-1.3$ with a scaling exponent of 2.9, yields a fractal dimension of $D_{SLR} = 1.52-1.62$ and a coefficient $b_{\tau S} = 2.7\ 10^4$ Pa, which is in accordance with previous values for CB and other lipid CMS systems (Awad et al., 2004; Vreeker et al., 1992). At higher crystal concentrations as measured by CR, the weak-link regime (WLR) is applicable. Since inter-crystal aggregate forces are *weaker* than intra-crystal aggregate forces, the scaling exponent is lower and originates from the inter-crystal aggregate bridges. The scaling exponent can be related to the fractal dimension as follows (Awad et al., 2004; Marangoni and McGauley, 2003; Narine and Marangoni, 1999; Shih et al., 1990; Vreeker et al., 1992):

$$\tau_0^{app} = b_{\tau W}\Phi_{SFC}^{1/(d-D)} \tag{5}$$

For $d = 3$, Equation (5) with a scaling exponent of 2.4, yields a fractal dimension of $D_{WLR} = 2.6$ and a coefficient $b_{\tau W} = 1.1\ 10^5$ Pa, which is in accordance with previous values for CB and other lipid CMS systems (Awad et al., 2004; Marangoni and McGauley, 2003; Vreeker et al., 1992). Comparing the two fractal dimensions leads to the conclusion that crystallization in laminar shear fields inhibits crystal growth in the 3 rd dimension, whereas under zero deformation conditions crystals aggregate into the 3rd dimension. The aggregation is indicated by the increase in apparent yield stress τ_0^{app} at constant Φ_{SFC}. Furthermore, the scaling exponent in the WLR is close to that of a Hertzian particle implying that the aggregates act as non-adhesive elastic spheres (Awad et al., 2004; Gross et al., 2014; Nordstrom et al., 2010). From the data presented in Fig. 1, a master curve of the relative viscosity $\eta_{rel} = \eta(\dot{\gamma})/\eta_{cont}$ as function of Φ_{SFC} for a fixed $\dot{\gamma}$ was obtained. The lowest high $\dot{\gamma}$ value for the UVP-PD measured samples was $\dot{\gamma} = 28\ s^{-1}$, whereas the highest low $\dot{\gamma}$ value for the CR measured samples was $\dot{\gamma} = 40\ s^{-1}$. Hence, extrapolation to $\dot{\gamma} = 40\ s^{-1}$ was performed for two samples (UVP-PD 1.7% and 2.7%). The continuous phase viscosity η_{cont} was measured with a concentric cylinder system yielding an Arrhenius function as depicted in Figure S6(B). From the CB CMS flow curves the relative viscosity at $\dot{\gamma} = 40\ s^{-1}$ ($\eta_{\dot{\gamma}=40s^{-1}}/\eta_{cont}$) was calculated and displayed in Fig. 3(B). For CB CMS measured directly after crystallization by UVP-PD, a fit according to Krieger and Dougherty (1959) was performed:

$$\eta_{rel} = \{1-(\Phi_{SFC}/\Phi_{max})\}^{-[\eta]\Phi_{max}} \tag{6}$$

The resulting values for $[\eta]$ and Φ_{max} were 20 and 0.17, respectively. Regarding the CB CMS measured by CR after zero deformation tempering, no Krieger-Dougherty relationship was observed. Instead, an empirical power-law fit of the form:

$$\eta_{rel} = b_\eta \Phi_{SFC}^h \tag{7}$$

with a coefficient $b_\eta = 1.3\ 10^4$ and a scaling exponent of $h = 2$ was performed. The master curves lead to the conclusion that the CB CMS in the SLR behaves like a suspension of anisotropic particles since $[\eta] > 2.5$ and $\Phi_{max} < 0.64$. Regarding suspensions where continuous and dispersed phase are of different chemical composition, $[\eta]$ and Φ_{max} are assumed constant since the suspended phase fraction and particle shape are constant for a given solvent quality (Vlassopoulos and Cloitre, 2014). In the case of CMS, $[\eta]$ and Φ_{max} are not constant, since the dispersed and continuous phase fraction are chemically identical and are related by a thermodynamic equilibrium between the liquid and solid phase. As a consequence, crystals may grow, aggregate and form links thereby reaching phase fractions up to values of $\Phi_{SFC} \approx 0.8$ for CB (Marangoni and McGauley, 2003). These underlying mechanisms of the thixotropic behavior of CB CMS are responsible for the limited validity of the Φ_{max} concept and the transition from a suspension to a jammed suspension. The transition from a suspension, where viscous and Brownian forces are at play, to a jammed suspension of elastic particles, where viscous and elastic forces are dominating is revealed by the change in scaling exponents and magnitude of the relative viscosity η_{rel}. Gross et al. (2014) found a similar scaling behavior for suspensions of jammed elastic particles at particle volume fractions > 0.64. Regarding the consistency factor K as presented in Fig. 3(C), the scaling exponent for the SLR was accessed by fitting the data with:

$$K = C_{kS} + b_{kS}\Phi_{SFC}^{\kappa S} \tag{8}$$

yielding $C_{kS} = 0.24$ Pa s^n, $b_{kS} = 1.39\ 10^2$ Pa s^n, $\kappa S = 2.0$. In the WLR, a fit of the form:

$$K = b_{kW}\Phi_{SFC}^{\kappa W} \tag{9}$$

was applied with $b_{kW} = 3.7\ 10^4$ Pa s^n and $\kappa W = 2.6$. In the WLR, the scaling exponent of K is higher compared to the scaling exponent of η_{rel}, whereas in the SLR the opposite is the case. Furthermore, the WLR shows a higher scaling exponent than the SLR which can be explained by transition from a suspension to a jammed suspension. The flow exponent n presented in 3(D) showed a master curve like behavior for the WLR as well as the SLR. A power-law fit of the form:

$$n = b_n\Phi_{SFC}^{\upsilon} \tag{10}$$

with a coefficient $b_n = 0.09$ and an exponent $\upsilon = -0.57$ was performed. In the SLR, n decreases steadily with increasing Φ_{SFC}, which is not the case in the WLR. In the WLR, n is reaching a plateau at ≈ 0.2 and is nearly independent of Φ_{SFC}. The low n values in the WLR are connected to the higher scaling exponents of K, since K and n could not be independently fitted. The values of n are in accordance with previous measurements of CB CMS where at $n \approx 0.2$ a plateau was reached (Birkhofer et al., 2008; Wassell et al., 2010; Young et al., 2008). Comparing CB CMS to other suspensions, only few systems reach similar low values for n (Wiklund and Stading, 2008). Systems which do reach similar values for n show high aspect ratios of the suspended particles (Ganani and Powell, 1985). So far, structural changes were deduced indirectly from scaling behaviors of rheological properties. Direct measurement of crystal morphology by AFM and PLM is a method to qualitatively assess structural changes in CB CMS. Fig. 4 shows AFM and PLM images of CB CMS directly after crystallization and after zero deformation tempering for 18 h. Fig. 4(A) and (B) show the morphology of a single crystal with a length of ≈ 2 μm, a width of ≈ 200 nm and a maximal height of ≈ 70–80 nm resulting in an aspect ratio > 10. From Fig. 4(B), a layered structure of the crystal becomes apparent. Directly after crystallization, small, anisotropic and weakly aggregated crystals are visible as depicted in Fig. 4(C). Fig. 4(D) shows strongly aggregated needle like crystals which form a network. The aggregated crystals show a decreased aspect ratio and increased overall size compared to the single crystal. Furthermore, the microscopy picture shows weak birefringence at the inter-aggregate bridges indicating thin layer thickness.

Fig. 4 confirms the structural changes as predicted by the scaling of τ_0, τ_0^{app} and η_{rel} as function of Φ_{SFC}. Directly after crystallization, the relative viscosity η_{rel} as function of Φ_{SFC} scales according to the model proposed by (Krieger and Dougherty, 1959) for anisotropic particles and the yield stress τ_0 according to the model proposed by (Shih et al., 1990). Both models derive the rheological response from the single particle shape and particle elastic constant. The derived $[\eta]$ and D_{SLR} are matching the high single crystal aspect ratio derived from Fig. 4(A) and (B). Fig. 4(C) and (D) reveal that the single crystals are weakly aggregated directly after crystallization inducing suspension like rheological response and that crystal aggregation is responsible for the transition to a jammed suspension rheological response as measured by the increase in fractal dimension D_{WLR} and decreased exponent of η_{rel} and τ_0^{app} as function of Φ_{SFC}. The thin layer between aggregates reveal the transition from the strong-into the weak link regime, where *inter*-aggregate forces are dictating the rheological response.

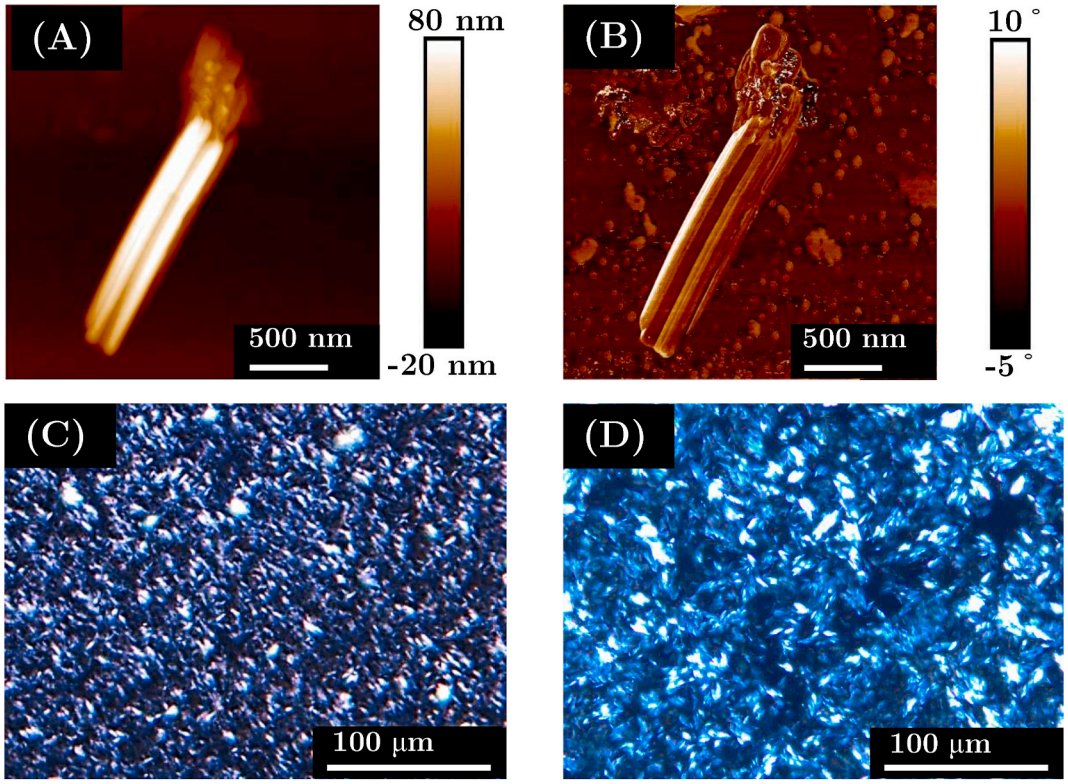

Fig. 4. AFM height (A) and phase (B) image of a single CB CMS crystal sampled directly after completion of the SeedMaster crystallization loop. PLM image of CB CMS sampled at the pipe exit of the direct crystallization set up (C) and after the completion of the SeedMaster crystallization loop with subsequent tempering for 18 h and 31.6 °C at zero deformation (D).

4. Conclusion

The shear rheology of CB CMS was investigated directly after SSHE crystallization by in-line UVP-PD and after zero deformation tempering by off-line CR and RR. It was found that the short measurement times t_M and continuous sample feed of the UVP-PD and CR method ensure identical deformation history for every probed shear rate $\dot{\gamma}$ and are thereby suited for thixotropic materials like CB CMS. UVP-PD was shown to probe at process relevant CB CMS deformation histories which is not necessarily the case for CR. The RR method was successfully used to quantify the thixotropic time scales relevant in CB CMS. Combining RR and CR results allows to transpose off-line generated rheological data to process relevant deformation histories offering a toolbox for food- and chemical process engineers. In order to identify the structural mechanisms responsible for CB CMS thixotropy, the (apparent) yield stress τ_0, τ_0^{app} and relative viscosity η_{rel} as function of Φ_{SFC} were derived and used to calculate the fractal dimension D and intrinsic viscosity $[\eta]$. Directly after crystallization, the CB CMS behaved like a suspension of weakly aggregated anisotropic particles with a calculated intrinsic viscosity of $[\eta] = 20$. The anisotropy originated from the crystallization under shear, which led to a fractal dimension of $D_{SLR} = 1.52 - 1.62$ indicating two-dimensional crystal growth and a scaling according to the SLR theory. After zero deformation tempering for 18 h, the fractal dimension increased to $D_{WLR} = 2.6$ due to aggregation of crystals into the 3rd dimension and a scaling according to the WLR theory. No intrinsic viscosity could be calculated since the relative viscosity did not scale according to (Krieger and Dougherty, 1959). PLM images revealed that the crystal aggregates were connected by thin inter-aggregate bridges converting the CB CMS to a jammed system. The scaling exponent of the apparent yield stress τ_0^{app} as function of crystal content is close to a Hertzian particle, indicating that the crystal aggregates can be seen as non-adhesive elastic particles.

Acknowledgement

The authors thank the Swiss National Science Foundation and Innosuisse for funding of the Bridge project 20B2-1-180971/1.

Appendix A. Supplementary data

Supplementary data to this article can be found online at https://doi.org/10.1016/j.jfoodeng.2021.110598.

Author statement

K. Mishra – Lab work, writing, data evaluation, data visualization, experimental planning, Lucas Kohler – Capillary rheology, lab work, Nico Kummer – AFM methodology, lab work, Simon Zimmermann – Lab work, Silas Ehrengruber – Lab work, Fabian Kämpf - Lab work, Damien Dufour – UVP-PD methodology consulting Gustav Nyström – AFM methodology consulting, P. Fischer – Writing, methodology, experiment conceptualization, Erich J. Windhab – Funding, writing, methodology, experiment conceptualization.

References

Andrae-Nightingale, L.M., Lee, S.Y., Engseth, N.J., 2009. Textural changes in chocolate characterized by instrumental and sensory techniques. J. Texture Stud. 40, 427–444. https://doi.org/10.1111/j.1745-4603.2009.00190.x.

Aronhime, J.S., Sarig, S., Garti, N., 1988. Dynamic control of polymorphic transformation in triglycerides by surfactants: the button syndrome. JAOCS (J. Am. Oil Chem. Soc.) 65, 1144–1150. https://doi.org/10.1007/BF02660571.

Awad, T.S., Rogers, M.A., Marangoni, A.G., 2004. Scaling behavior of the elastic modulus in colloidal networks of fat crystals. J. Phys. Chem. B 108, 171–179. https://doi.org/10.1021/jp036285u.

Bertsch, P., Savorani, L., Fischer, P., 2019a. Rheology of Swiss cheese fondue. ACS Omega 4, 1103–1109. https://doi.org/10.1021/acsomega.8b02424.

Bertsch, P., Schneider, L., Bovone, G., Tibbitt, M.W., Fischer, P., Gstöhl, S., 2019b. Injectable biocompatible hydrogels from cellulose nanocrystals for locally targeted

sustained drug release. ACS Appl. Mater. Interfaces 11, 38578–38585, 10.1021/acsami.9b15896. https://pubs.acs.org/doi/10.1021/acsami.9b15896.
Birkhofer, B.H., Jeelani, S.K., Windhab, E.J., Ouriev, B., Lisner, K., Braun, P., Zeng, Y., 2008. Monitoring of fat crystallization process using UVP-PD technique. Flow Meas. Instrum. 19, 163–169. https://doi.org/10.1016/j.flowmeasinst.2007.08.008.
Bolliger, S., Breitschuh, B., Stranzinger, M., Wagner, T., Windhab, E., 1998. Comparison of precrystallization of chocolate. J. Food Eng. 35, 281–297. https://doi.org/10.1016/S0260-8774(98)00046-6.
Breitschuh, B., Windhab, E.J., 1996. Direct measurement of thermal fat crystal properties for milk-fat fractionation. JAOCS (J. Am. Oil Chem. Soc.) 73, 1603–1610. https://doi.org/10.1007/BF02523532.
Chapman, G.M., Akehurst, E.E., Wright, W.B., 1971. Cocoa butter and confectionery fats. Studies using programmed temperature X-ray diffraction and differential scanning calorimetry. J. Am. Oil Chem. Soc. 48, 824–830. https://doi.org/10.1007/BF02609292.
Flaud, P., Bensalah, A., Peronneau, P., 1997. Deconvolution process in measurement of arterial velocity profiles via an ultrasonic pulsed Doppler velocimeter for evaluation of the wall shear rate. Ultrasound Med. Biol. 23, 425–436. https://doi.org/10.1016/S0301-5629(96)00200-1.
Ganani, E., Powell, R., 1985. Suspensions of rodlike particles: literature review and data correlations. J. Compos. Mater. 19, 194–215. https://doi.org/10.1177/002199838501900301.
Grob, L., Papadea, K., Braun, P., Windhab, E.J., 2021. In-line detection method for crystallization, contraction and mold detachment during cooling of confectionery products. J. Food Eng. 292, 110322. https://doi.org/10.1016/j.jfoodeng.2020.110322.
Gross, M., Krüger, T., Varnik, F., 2014. Rheology of dense suspensions of elastic capsules: normal stresses, yield stress, jamming and confinement effects. Soft Matter 10, 4360. https://doi.org/10.1039/c4sm00081a.
Herschel, W.H., Bulkley, R., 1926. Konsistenzmessungen von gummi-benzollösungen. Kolloid Z. 39, 291–300. https://doi.org/10.1007/BF01432034.
Jorgensen, J.E., Garbini, J.L., 1974. An analytical procedure of calibration for the pulsed ultrasonic Doppler flow meter. J. Fluid Eng. 96, 158–167. https://doi.org/10.1115/1.3447122.
Kagiyama, M., Ogasawara, Y., Tadaoka, S., Kajiya, F., 1999. Measurement accuracy of the flow velocity in pulsed ultrasound Doppler velocimeter. Ultrasound Med. Biol. 25, 1265–1274. https://doi.org/10.1016/S0301-5629(99)00082-4.
Koyano, T., Hachiya, I., Sato, K., 1990. Fat polymorphism and crystal seeding effects on fat bloom stability of dark chocolate. Food Struct. 9, 231–240. https://digitalcommons.usu.edu/foodmicrostructure/vol9/iss3/6.
Krieger, I.M., Dougherty, T.J., 1959. A mechanism for non-Newtonian flow in suspensions of rigid spheres. Trans. Soc. Rheol. 3, 137–152. https://doi.org/10.1122/1.548848.
Macias-Rodriguez, B.A., Ewoldt, R.H., Marangoni, A.G., 2018. Nonlinear viscoelasticity of fat crystal networks. Rheol. Acta 57, 251–266. https://doi.org/10.1007/s00397-018-1072-1.
Macias-Rodriguez, B.A., Marangoni, A.G., 2018. Linear and nonlinear rheological behavior of fat crystal networks. Crit. Rev. Food Sci. Nutr. 58, 2398–2415. https://doi.org/10.1080/10408398.2017.1325835.
Marangoni, A.G., McGauley, S.E., 2003. Relationship between crystallization behavior and structure in cocoa butter. Cryst. Growth Des. 3, 95–108. https://doi.org/10.1021/cg025580l.
Marangoni, A.G., Rogers, M.A., 2003. Structural basis for the yield stress in plastic disperse systems. Appl. Phys. Lett. 82, 3239–3241. https://doi.org/10.1063/1.1576502.
Mishima, S., Suzuki, A., Sato, K., Ueno, S., 2016. Formation and microstructures of whipped oils composed of vegetable oils and high-melting fat crystals. JAOCS (J. Am. Oil Chem. Soc.) 93, 1453–1466. https://doi.org/10.1007/s11746-016-2888-4.
Mishra, K., Bergfreund, J., Bertsch, P., Fischer, P., Windhab, E.J., 2020a. Crystallization-induced network formation of tri- and monopalmitin at the middle-chain triglyceride oil/air interface. Langmuir 36, 7566–7572, 10.1021/acs.langmuir.0c01195. https://pubs.acs.org/doi/10.1021/acs.langmuir.0c01195.
Mishra, K., Dufour, D., Windhab, E.J., 2020b. Yield stress dependent foaming of edible crystal-melt suspensions. Cryst. Growth Des. 20, 1292–1301. https://doi.org/10.1021/acs.cgd.9b01558.
Narine, S.S., Marangoni, A.G., 1999. Fractal nature of fat crystal networks. Phys. Rev. 59, 1908–1920. https://doi.org/10.1103/PhysRevE.59.1908.
Nordstrom, K.N., Verneuil, E., Arratia, P.E., Basu, A., Zhang, Z., Yodh, A.G., Gollub, J.P., Durian, D.J., 2010. Microfluidic rheology of soft colloids above and below jamming. Phys. Rev. Lett. 105, 175701. https://doi.org/10.1103/PhysRevLett.105.175701.
Padar, S., Mehrle, Y.E., Windhab, E.J., 2009. Shear-induced crystal formation and transformation in cocoa butter. Cryst. Growth Des. 9, 4023–4031. https://doi.org/10.1021/cg900194t.
Pérez-Martínez, D., Alvarez-Salas, C., Charó-Alonso, M., Dibildox-Alvarado, E., Toro-Vazquez, J., 2007. The cooling rate effect on the microstructure and rheological properties of blends of cocoa butter with vegetable oils. Food Res. Int. 40, 47–62. https://doi.org/10.1016/j.foodres.2006.07.016.
Sebben, D.A., Gao, N., Gillies, G., Beattie, D.A., Krasowska, M., 2019. Fractionation and characterisation of hard milk fat crystals using atomic force microscopy. Food Chem. 279, 98–104. https://doi.org/10.1016/j.foodchem.2018.11.136.
Shih, W.H., Shih, W.Y., Kim, S.I., Liu, J., Aksay, I.A., 1990. Scaling behavior of the elastic properties of colloidal gels. Phys. Rev. 42, 4772–4779. https://doi.org/10.1103/PhysRevA.42.4772.
Stranzinger, M., Bieder, A., Feigl, K., Windhab, E., 2002. Effects of flow incidence and secondary mass flow rate on flow structuring contributions in scraped surface heat exchangers. J. Food Process. Eng. 25, 159–187. https://doi.org/10.1111/j.1745-4530.2002.tb00561.x.
Stranzinger, M., Feigl, K., Windhab, E., 2001. Non-Newtonian flow behaviour in narrow annular gap reactors. Chem. Eng. Sci. 56, 3347–3363. https://doi.org/10.1016/S0009-2509(01)00039-2.
Svanberg, L., Ahrné, L., Lorén, N., Windhab, E., 2013. Impact of pre-crystallization process on structure and product properties in dark chocolate. J. Food Eng. 114, 90–98. https://doi.org/10.1016/j.jfoodeng.2012.06.016.
Timms, R., 1984. Phase behaviour of fats and their mixtures. Prog. Lipid Res. 23, 1–38. https://doi.org/10.1016/0163-7827(84)90004-3.
Vlassopoulos, D., Cloitre, M., 2014. Tunable rheology of dense soft deformable colloids. Curr. Opin. Colloid Interface Sci. 19, 561–574. https://doi.org/10.1016/j.cocis.2014.09.007.
Vreeker, R., Hoekstra, L., den Boer, D., Agterof, W., 1992. The fractal nature of fat crystal networks. Colloid. Surface. 65, 185–189. https://doi.org/10.1016/0166-6622(92)80273-5.
Wassell, P., Wiklund, J., Stading, M., Bonwick, G., Smith, C., Almiron-Roig, E., Young, N.W.G., 2010. Ultrasound Doppler based in-line viscosity and solid fat profile measurement of fat blends. Int. J. Food Sci. Technol. 45, 877–883. https://doi.org/10.1111/j.1365-2621.2010.02204.x.
Wiklund, J., Stading, M., 2008. Application of in-line ultrasound Doppler-based UVP-PD rheometry method to concentrated model and industrial suspensions. Flow Meas. Instrum. 19, 171–179. https://doi.org/10.1016/j.flowmeasinst.2007.11.002.
Wille, R.L., Lutton, E.S., 1966. Polymorphism of cocoa butter. JAOCS (J. Am. Oil Chem. Soc.) 43, 491–496. https://doi.org/10.1007/BF02641273.
Windhab, E., 1988. A new method for describing the time-dependent rheological behaviour of concentrated suspensions. In: Progress and Trends in Rheology II. Steinkopff, Heidelberg, pp. 317–320. https://link.springer.com/chapter/10.1007/978-3-642-49337-9_108.
Young, N.W.G., Wassell, P., Wiklund, J., Stading, M., 2008. Monitoring struturants of fat blends with ultrasound based in-line rheometry (ultrasonic velocity profiling with pressure difference). Int. J. Food Sci. Technol. 43, 2083–2089. https://doi.org/10.1111/j.1365-2621.2008.01826.x.